Combining first-principles kinetics and experimental data to establish guidelines for product selectivity in electrochemical $CO_{(2)}$ reduction

Georg Kastlunger*,† Hendrik H. Heenen,†,‡ and Nitish Govindarajan*,†

†*Catalysis Theory Center, Department of Physics, Technical University of Denmark (DTU), 2800 Kgs. Lyngby, Denmark*

‡*Fritz-Haber-Institut der Max-Planck-Gesellschaft, D-14195 Berlin, Germany*

E-mail: geokast@dtu.dk

Abstract

The electrochemical reduction of $CO_{(2)}$ is envisioned as one of the most promising ways to close the industrial carbon cycle by producing high value chemicals and fuels using renewable electricity. Although the performance of CO_2 electrolyzers have improved substantially in the last decade, they still suffer from poor selectivity towards the most desired products, ethylene and ethanol. This is, in part due to the fact that a detailed mechanistic understanding of the selectivity towards various products is still lacking, although necessary for process optimization. Herein, we perform microkinetic simulations based on constant potential density functional theory to elucidate the reaction pathways for $CO_{(2)}$ electroreduction on Cu towards the major multi-carbon products. We find that ethylene is the first product that bifurcates from the oxygenates, followed by acetate. Acetaldehyde is a direct intermediate in the production of ethanol.

We provide atomistic level insights on the major role played by the electrode potential and electrolyte pH in determining the selectivity towards ethylene, oxygenates and methane, and relate the origin of the selectivity to general trends in electrochemical reaction energetics. Finally, we compare the results of our microkinetic simulations to an experimental database of previously reported measurements and suggest guidelines for improving the selectivity towards the specific products. Our study paves the way for the design of efficient CO_2 electrolyzers for the production of targeted multi-carbon products, thereby moving a step closer towards their widespread adaptation.

Introduction

Globally increasing temperatures and climatic anomalies demand means for reducing greenhouse gases in the atmosphere.[1] Electrochemical $CO_{(2)}$ reduction ($eCO_{(2)}R$) is considered as a promising route to close the anthropogenic carbon cycle by converting a major waste gas into high value fuels and chemicals using renewable electricity.[2,3] Substantial advancements in the design of $CO_{(2)}$ electrolyzers have been made recently,[4–7] approaching industrially relevant current densities.[6,8] However, with the exception of the $2e^-$ products, carbon monoxide[9–11] and formate,[12,13] the large palette of simultaneously produced chemicals beyond $2e^-$ products within $eCO_{(2)}R$ and the ubiquitous competition with the hydrogen evolution reaction (HER) hinders commercialization and creates the need to couple electrolyzers to costly separation techniques.[14] Thus, it is essential to improve the intrinsic selectivity towards the desired high-value products, such as ethylene and ethanol, in order to make $eCO_{(2)}R$ an economically viable process for CO_2-valorization.

Copper, the only monometallic catalyst known to produce significant amounts of multi-carbon $eCO_{(2)}R$ products (C_{2+}-products),[3,15,16] has been studied extensively and a wide-range of experiments have attempted to improve the selectivity towards specific products.[15,17–30] Some examples of methods that have been used to influence the product selectivity on Cu electrodes consist of: altering specific surface morphology,[22,26,31] doping or alloying

Cu[19,25,32–35] and systematically changing the oxidation state of Cu.[28,36] However, the long term stability of engineered Cu surfaces under reaction conditions is not guaranteed[37] and a direct comparison of electrodes with varying surface morphologies taking into account the electrochemical active surface area (ECSA) shows that the improvements in intrinsic activity and selectivity towards specific products achieved by the aforementioned means are moderate.[3,38–40] Beyond modifying the electrode using the aforementioned methods, we argue that parameters custom to electrochemical processes (i.e. the applied potential and electrolyte environment) should be taken into account when exploring the dependence of product selectivity on the electrolyzer setup. The applied potential and the electrolyte composition are powerful tools to alter the activity of catalytic reactions by orders of magnitude,[38] analogous to (but much more powerful than) temperature and pressure in thermal catalysis.[41]

From a modeling standpoint, detailed mechanistic studies on the effect of the applied potential and electrolyte pH on the product distribution in $eCO_{(2)}R$ are complicated due to the multitude of possible reaction intermediates, the large number of reaction steps towards the desired products and the need to estimate potential-dependent reaction kinetics at constant potential in acidic, neutral and alkaline conditions. In particular, the need for simulating potential-dependent activation barriers with H_2O as the proton donor has resulted in a methodological bottleneck as conventional transition state searches at constant charge conditions mostly result in the adsorption of the OH^--ion produced during the reaction, resulting in the overall reaction being non-electrochemical.[42]

As a result of these challenges, previous mechanistic studies are mostly focused on the identification of thermodynamically feasible reaction pathways[25,43–47] or kinetic analyses performed in acidic conditions at constant charge (where H_3O^+ ions are used as the proton donor),[48–50] although $eCO_{(2)}R$ is exclusively performed in neutral or alkaline conditions. Furthermore, symmetry factors[51,52] (i.e the potential response of the activation barrier in elementary steps) are assumed to be 0.5 in most studies ,[48,49] although it has been shown in recent studies that the symmetry factors do not have any preference for such cardinal

values[53,54] and are dependent on the identity of the reacting species.[55] The simplification of assuming a constant and equal potential response for the elementary reaction steps neglects any variations that can occur in the preferred reaction pathways due varying potential and electrolyte pH.

In this work, we present a constant potential DFT[56–61]-based study on the reaction mechanisms towards C_{2+}-products for $eCO_{(2)}R$ on Cu(100), which we recently identified as the most active Cu facet for the production of C_{2+}-productsusing constant potential DFT based microkinetic simulations.[62] By incorporating the calculated reaction energetics for $eCO_{(2)}R$ (including kinetics) in neutral/alkaline conditions into microkinetic simulations, we are able to capture the changes in selectivity of the C_{2+}-products with variations in the applied potential and electrolyte pH. We also benchmark our identified mechanistic conclusions on the selectivity of C_{2+}-products by analyzing general trends in the activation barriers and potential responses for specific electrochemical elementary reaction steps involving carbon and oxygen species. Furthermore, we evaluate the predictions from the microkinetic simulations by comparing our predicted selectivity trends in C_{2+}-products with a curated database on previously reported $eCO_{(2)}R$ experiments on Cu electrodes and find good agreement. Finally, based on our detailed mechanistic insights, we are able to propose general guidelines for the working conditions of CO_2 electrolyzers to steer the selectivity towards the desired C_{2+}-products.

Results and Discussion

The reaction thermodynamics of $eCO_{(2)}R$ alone does not provide conclusive mechanistic insights

In order to obtain an initial understanding of the free energy landscape of $eCO_{(2)}R$ towards C_{2+}-products, we calculated the (constant-potential) formation free energies of reaction intermediates (denoted as ΔG^{ϕ}) starting from adsorbed CO towards the $8e^-$-products

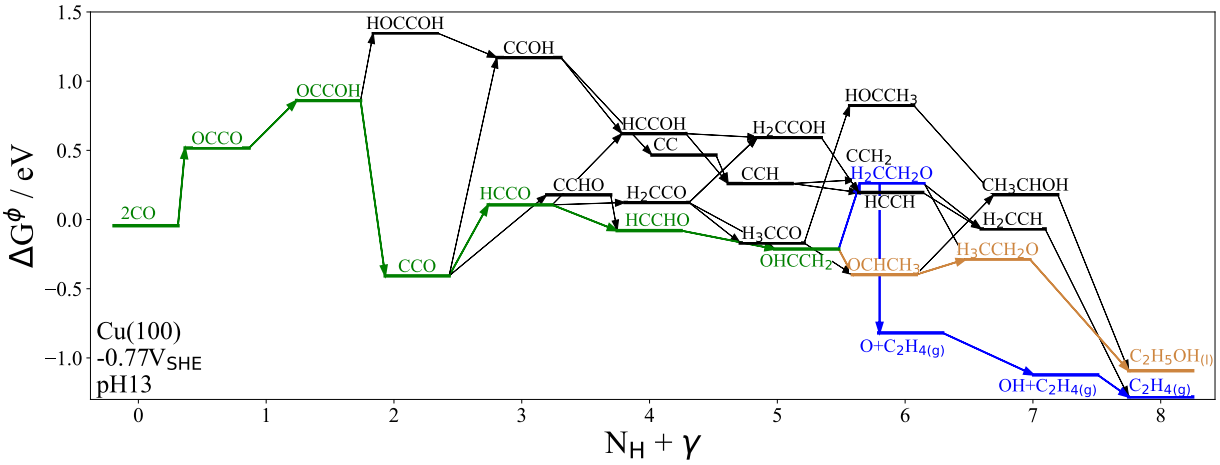

Figure 1: Free energy profile towards ethylene and ethanol at $0V_{RHE}$ and pH 13 on Cu(100). A wide but not complete selection of possible adsorbed reaction intermediates is shown. The thermodynamically preferred reaction paths are highlighted with green intermediates, symbolizing the most stable intermediates shared by both products, blue steps, referring to the reaction path to ethylene and ochre steps leading towards ethanol. Note that the x-axis contains both the number of transferred proton-electron pairs (N_H) and the intermediate's respective potential sensitivity (γ).[62] We provide schematics of the atomic structures of each intermediate in figure S1Legend for the intermediate structure noted in Figure 1 of the main artice. Note that in the actual calculation a water bilayer was included in each of the simulation cells.figure.caption.2

ethylene and ethanol, shown in Figure 1. Note that the effective potential response of the intermediates (denoted in the x-axis) deviates from integer values, as a consequence of the intermediates' specific potential response(γ), arising from the (theoretical) potentiostats' need to counter a surface dipole upon the formation of these intermediates, which we described in detail in a recent work.[62] We have already performed a first selection of relevant reaction intermediates in our analysis, based on conclusions from our previous mechanistic study where we identified the mechanism towards C_{2+}-products to proceed via the *CO dimerization step and subsequent protonation of the *OCCO dimer to *OCCOH at typical reaction conditions relevant to $eCO_{(2)}R$.[62] These conclusions are also in agreement with several previous studies .[25,43–47] Thus, all intermediates that can only be formed from the *CHO, *COH and *OCCHO species have been excluded in the present work. In addition, intramolecular rearrangements of the intermediates have also not been considered as they would likely be energetically unfavourable. The above mentioned selection criteria lead to a strongly reduced, albeit still a large number of possible reaction intermediates. Upon *CO dimerization to form *OCCOH, the terminal oxygen can be protonated to form a bidentate *HOCCOH species or the -OH group can desorb to form *CCO, the latter having substantially favourable reaction thermodynamics (cf. Figure 1). In the case of *HOCCOH, only the desorption of OH^- to form *CCOH is a reasonable reaction step, as the steric hinderance and a partial positive charge makes the protonation of the carbon atom unlikely. *CCO on the other hand, is readily accessible to protons from the solvent on all three atoms of the adsorbate. Thus, we include all three intermediates resulting from the protonation of *CCO, namely *HCCO,*CCHO,*CCOH in Figure 1. Following these PCET steps, a multitude of elementary reactions are possible towards the formation of ethylene and ethanol.

We highlight the preferred pathways based on reaction thermodynamics towards ethanol and ethylene in Figure 1 (green, blue and ochre). In these reaction mechanisms, the C_{2+}-products share a common reaction pathway, shown in green, up to $*OHCCH_2$. The pathway towards ethylene, shown in blue, then proceeds via $*H_2CCH_2O$, from which it desorbs and

the resulting *O is further reduced to H_2O via two PCET steps in order to close the catalytic cycle for ethylene-formation. *H_2CCH_2O has been proposed as the crucial intermediate towards both ethylene and ethanol before,[43,63–65] as acetaldehyde (acetaldehyde) spontaneously desorbs from Cu terraces during DFT based geometry optimizations. We do, however, argue that it was clearly shown that feeding acetaldehyde ($OCHCH_3$) in $eCO_{(2)}R$ experiments leads to a substantial increase in ethanol production,[66,67] making acetaldehyde a possible reaction intermediate towards ethanol. Indeed, we find the pathway via acetaldehyde to be the most stable reaction pathway towards ethanol, as shown in ochre in Figure 1. Independent of *H_2CCH_2O or acetaldehyde being the relevant intermediates towards ethanol, the final intermediate leading to ethanol is *H_3CCH_2O.

The most stable reaction pathways towards ethylene and ethanol identified in this work are in good agreement with previous studies.[3,43,63–65,68] However, we argue that there is indeed no justification to assume that the most favourable reaction pathway solely based on reaction thermodynamics is the preferred pathway for the production of C_{2+}-products. In fact, at typical reaction conditions during $eCO_{(2)}R$ (i.e. below -1V_{SHE} and at neutral or alkaline pH), nearly all reaction steps are exergonic (cf. figure S3Free energy diagram at representative condition for CO reduction. Note that almost all reaction steps are exergonic, hence not allowing to distinguish between reasonable reaction pathways.figure.caption.9). Therefore, it is crucial to estimate the reaction kinetics involved in the formation of the various reaction intermediates to identify the preferred reaction pathways towards ethylene and ethanol.

Reaction kinetics reveal that a competition between the protonation of C and O is central to product selectivity

In order to find the most likely reaction pathways towards ethylene and ethanol based on the free energy profile shown in figure 1, we performed constant potential nudged elastic band (NEB) calculations[69] to estimate activation barriers in neutral/alkaline conditions using the

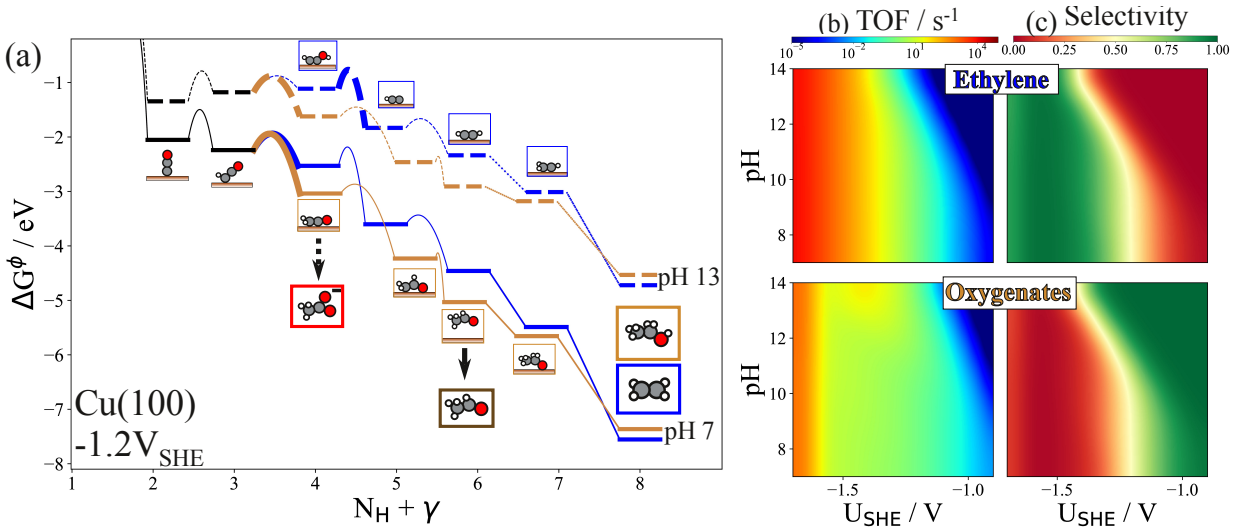

Figure 2: Determined (a) free energy pathways,(b) turnover frequencies (TOF's) and (c) selectivity to ethylene and oxygenate products determined from combining thermodynamics and alkaline reaction kinetics along the reaction network.

Solvated Jellium Method (SJM)[59] with H_2O as the proton donor (See the computational methods section for details on the setup). Our strategy consisted of a step-by-step estimation of the activation barriers along the reaction pathway and performing microkinetic simulations after each elementary step in order to understand the dominant pathway towards the desired products. The identified reaction pathways towards ethylene, ethanol, acetate and acetaldehyde based on our kinetic analysis is shown in Figure 2(a), while we describe all the competing elementary steps in detail in the SI section 3Detailed stepwise kinetic studysection.3.

We find that the kinetically favoured pathway towards ethylene and oxygenates is shared after *CO-dimerization and subsequent protonation steps to form *OCCOH,[62] *CCO and *HCCO. We identify the protonation of *HCCO as the major selectivity determining step (SDS), as we observe a bifurcation in the reaction pathways towards ethylene and oxygenates after this step. At this reaction step the protonation of the oxygen atom leads to the production of ethylene, while the protonation of the terminal-carbon atom leads to the production of the oxygenate products including acetaldehyde acetate and ethanol.

The pathway towards ethylene proceeds from *HCCOH through *HCC by OH^--desorption,

followed by subsequent protonation of *HCC until ethylene is produced as a final product. At neutral pH, the protonation of *HCCO on the O-end defines the activation barrier towards ethylene starting from the last common intermediate of the forking pathways (*HCCO). However, with an increase in pH the unfavourable thermodynamics of *HCCOH leads to the desorption of OH^- from *HCCOH to become the selectivity determining step (i.e. the highest barrier after the last common intermediate).

As described in detail in a recent study,[40] we identified the step from *HCCO to *H_2CCO to be a combination of the desorption of *HCCO as an anion followed by subsequent protonation in solution. This was a natural outcome of our transition state search for this step and is crucial for explaining the selectivity behaviour of acetate, as it is formed in solution by a nucleophilic attack of H_2O or OH^- on H_2CCO. Instead of leading to the production of acetate, H_2CCO can readsorb on the catalyst surface and be protonated to form *H_2CCHO. We found that *H_2CCHO is very weakly bound to the catalyst surface and its desorption as an anion, which we show in detail in figure S9Reaction band and charge transfer (change of number of electrons in the unit cell) for the elementsry step from *OHCCH2 to acetaldehyde. Note that *OHCCH2 desorbs first and most of the charge transfer happens in that step. This behvaiour also leads to the protonation barrier in solution to be independent of potential (represented by varying workfunctions (WF).figure.caption.15, is thermodynamically favoured and nearly activationless at potentials below -1V_{SHE} . Thus, *H_2CCHO desorbs from the surface and forms acetaldehyde in solution. The latter can either diffuse into bulk solution or readsorb on the catalyst surface to be further reduced towards ethanol.

We developed a microkinetic model based on the energetics shown in Figure 2(a). The identified activity and selectivity behaviour of the complete mechanisms towards ethylene and oxygenates with potential and electrolyte pH are shown in Figure 2(b) and (c), where we define the selectivity to product i among all C_{2+}-products as

$$S_i^{C_{2+}} = \frac{TOF_i}{\sum_k^{C_{2+}} TOF_k}. \tag{1}$$

Note that, we did not include the mechanisms to acetate and acetaldehyde in the microkinetic model, as they are strongly influenced by mass transport limitations, which are not explicitly accounted for in our microkinetic simulations. Instead, we assume all acetate and acetaldehyde to get converted to ethanol and thereby effectively distinguish only ethylene vs. oxygenate selectivity.

Interestingly, both potential and the electrolyte pH are predicted to influence the relative selectivity between the products, leading to the production of oxygenates being preferred at high pH and low overpotentials (green area in Figure 2(c) lower panel), while the total rate towards C_{2+}-products (sum of TOFs in figure 2(b)) is unaffected by the pH (cf. figure S10Total rate towards C_{2+}-products resulting from the applied microkinetic model. figure.caption.16). We also performed a degree of selectivity control analysis (DSC) in figure S4Degree of Selectivity control analysis within the microkinetic model performed for the mechanisms described in the main article. All reaction intermediates and barriers were included in the analysis. However, only intermediates and barriers with a numerical value DSC above 0.1 were included in the plot. The labels H-HCCO, HCC-OH and HCCO-H refer to the elementary reaction transitions states HCCO+H2O+e^- $\rightarrow$$H_2CCO$+$OH^-$, HCCO+$H_2O$+$e^-$ $\rightarrow$HCCOH+OH^-, HCCOH+e^- $\rightarrow$HCC+OH^-, respectively.figure.caption.10, which allows the identification of the elementary steps that control the product selectivity, and reflects our interpretation of the free energy diagrams in figure 2(a).

The effect of the potential on the product selectivity (up to pH $\approx$ 11) predicted by the microkinetic simulation (cf. Figure 2(c)) is a consequence of the larger energetic response of the transition state *HCCO-H to a change in potential compared to the transition state *H-HCCO, calculated as 0.77 and 0.49, respectively. Although all discussed C_{2+}-products share a common rate limiting step (RLS), this difference in effective potential response of the barriers (α) at the SDS leads to deviations in the effective α towards the respective products. As we derive in the SI section 6Derivation of the potential and pH response for specific productssection.6, the effective α towards a product A sharing a SDS with a product

B takes the form:

$$\alpha_{\mathrm{A}} = \alpha_{\mathrm{RLS}} + (1 - S_A)(\alpha_{\mathrm{A,SDS}} - \alpha_{\mathrm{B,SDS}}) \tag{2}$$

where α_{RLS} refers to the transfer coefficient of the RLS, $\alpha_{\mathrm{A,SDS}}$ is the transfer coefficient towards product i with respect to last reaction intemediate shared with B. Note that α_{A} is potential dependent which propagates into measured Tafel slopes being defined as $-\frac{\ln 10 \mathrm{k_B} T}{\mathrm{e}\alpha_A}$. From equation 2, we conclude that α_A corresponds to α_{RLS} if A is the majority product ($\mathrm{S}_A \rightarrow 1$). In the case of A being the minority product (S_A ¡¡ 1) α_A on the other hand is dependent on the relationship of the transfer coefficient after the SDS. Furthermore, equation 2 emphasizes that if the product distribution changes with potential, one can expect variations in the Tafel slopes.

In the determined selectivity behaviour below pH 11, as the SDS is comprised of two elementary steps starting from the same reactant (*HCCO), we do not expect to observe a pH dependence in the selectivity. However, above pH 11, our simulations show a pH dependence in the selectivity.

The source of the observed pH-dependence in selectivity is due to the suppression of ethylene relative to ethanol at high pH, while the overall rate towards C_{2+}-products is pH independent. This suppression of ethylene is as a consequence of the activation energy to form *HCC (via *HCC-OH dissociation) being located one step after the actual SDS. Thus, reaching *HCC-OH needs one more proton than reaching *H-HCCO, the relevant intermediate towards oxygenates. As a result, *HCC-OH is destablized with increasing pH compared to *H-HCCO..[50,62]

Thus, starting from the model in equation 2 again, we also derived the pH dependence towards a specific products as

$$\frac{\partial \log \mathrm{TOF_A}}{\partial pH} = -N_{\mathrm{H,RLS}} - (1 - S_{\mathrm{A}})(N_{\mathrm{H,B}} - N_{\mathrm{H,A}}) \tag{3}$$

with $N_{H,RLS}$ referring to the number of protons transferred up to the RLS and $N_{H,i}$ being the number of protons transferred until reaching the effective barrier towards product i, starting from the last common intermediate for all products (*HCCO in our case). Equation 3 shows that if $N_{H,A}$=$N_{H,B}$ the pH dependence toward all products involved in the SDS is the same as that of the RLS. Thus, in such a case, analogous to the found behaviour up to pH 11, we expect to have no change in selectivity with pH. In the case above pH 11, however, $N_{H,*HCC-OH}$=$N_{H,*H-HCCO}$+1, leading to a pH-dependence in the selectivity between ethylene and oxygenates.

The identified behaviour suggests a design principle for $eCO_{(2)}R$ electrolyzers, namely that if a high ethylene-yield is desired the pH should not exceed a value of 11 or otherwise the electrolyzer has to be operated at sufficiently high overpotentials in order to benefit from the stronger potential response of *HCCO-H at the SDS. We note in passing that the estimated potential response is an outcome of static transition state searches, and we therefore advocate for further benchmarking of these observations in future studies. In the following, we will show that the observed behaviour of the potential response in alkaline $eCO_{(2)}R$can be based on general trends in proton transfer reaction energetics.

The change in product selectivity with potential is based on general trends in reaction energetics

The competition between reaction thermodynamics and kinetics in the electrochemical formation or breaking of specific bonds (C-H, O-H,-OH) are the central aspects of the identified potential and pH-dependence in the selectivity of the various C_{2+}-products outlined in the previous section.

Figure 3(a) shows the identified Brønsted-Ewald-Polanyi (BEP) relationships of the three major reaction types relevant for $eCO_{(2)}R$ (C-protonation, O-protonation and OH-desorption). Our results show that the formation of C-H bonds (C-protonation, brown markers) is generally preferred thermodynamically over the formation of O-H bonds (O-

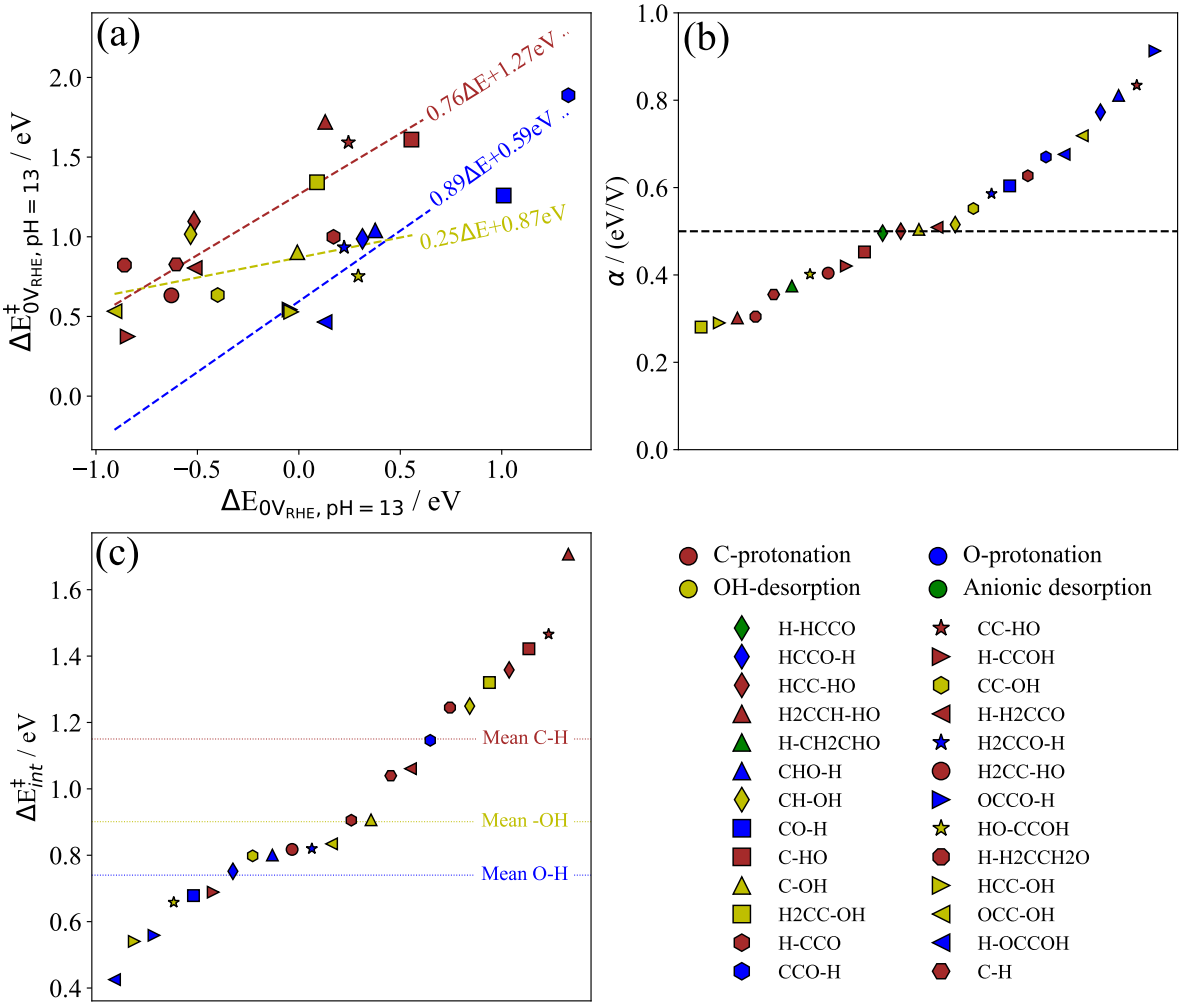

Figure 3: Identified general trends in thermodynamics and kinetics, namely (a) the BEP relationship at $0V_{RHE}$ and pH 13, (b) the potential response of the transition states (α) and (c) the determined reaction barriers at thermoneutral reaction conditions ($\Delta E^{\ddagger}_{int}$). In all panels the various reaction-types are distinguished by varying colors.

protonation, blue markers), as can be seen by the former's relative shift to the left (on the x-axis) with respect to the latter. However, we find the opposite behaviour for reaction kinetics, namely at a given ΔE, $\Delta E^{\ddagger}$ (the activation barrier) for C-H bond formation is increased by ca.0.7 eV compared to O-H bond formation. Thus, the BEP-relationships show comparable slopes of ≈ 0.8, but an increase in the intercept for C-protonation (1.27 eV) over O-protonation (0.59 eV). The combination of the observed behaviour in reaction thermodynamics and kinetics leads to comparable $\Delta E^{\ddagger}$ at $0V_{RHE}$ and pH 13 for C-H and O-H, represented by the comparable $\Delta E^{\ddagger}$ values in figure 3(a). These results point to the fact that a priori predictions of the preference for a given reaction step are not possible.

Note that in the context of electrochemical reaction steps in neutral/alkaline conditions, the BEP relationship needs to be determined at a given potential and pH, as activation barriers ($\Delta E^{\ddagger}$, y-axis in Figure 3(a)) are only dependent on the absolute potential, while the reaction energies (ΔE, x-axis in Figure 3(a)) are dependent on both the potential and pH. This behaviour changes in acidic conditions, where both activation barriers and reaction energies exhibit equal pH-dependence.[49,62] Furthermore, we note that elementary reactions not directly relevant to the mechanism towards C_{2+}-products but computed in course of this work were also included in Figure 3 in order to increase the sample size of reactions in the analysis.

The reaction steps involving the anionic desorption of an OH-group (OH-desorption), shown as yellow markers in Figure 3(a), are thermodynamically more favourable than the steps involving O-H bond formation, while we do not observe any obvious trend in the comparison to the steps involving C-H bond formation. We posit that this might be due to a small number of relevant -OH desorption reactions included within the studied mechanism. Interestingly, we determined a minor dependence of $\Delta E^{\ddagger}$ on ΔE for steps involving OH-desorption.

As stated earlier, the BEP-relationships at a given potential (and pH) alone do not allow for a straight-forward estimation of the kinetic preferences towards specific reaction types.

The change of $\Delta E^{\ddagger}$ with potential, α, shown in Figure 3(b), on the other hand shows a clear trend of the steps involving O-H bond formation (i.e. O-protonation) exhibiting a stronger response to the applied potential (i.e. α) compared to steps involving C-H bond formation (i.e. C-protonation). In all investigated elementary steps, O-H exhibited $\alpha > 0.5$, which we attribute to the more endergonic nature of the O-H bond formation step. The unfavourable ΔE leads to a transition state being located later in the reaction path, thus resulting in a larger α.[70] In contrast, the C-H reaction steps that are mostly exergonic exhibited $\alpha \leq 0.5$, as consequence of their transition states being located earlier in the reaction path within the transition state search. Similar to the absolute $\Delta E^{\ddagger}$ at a given reaction condition, the α of OH-desorption also does not show a clear trend compared to the other two reaction types in Figure 3(b) and lies somewhat in between the estimated α values for the C-H and O-H protonation steps.

The absolute difference at fixed reaction conditions and potential responses can be combined in the determination of the intrinsic $\Delta E^{\ddagger}$ ($\Delta E^{\ddagger}_{int}$), the activation energy at the potential where $\Delta E=0$, shown in Figure 3(c). Note that, analogous to Figure 3(a), the intrinsic barriers are pH dependent, as ΔE is pH dependent, while $\Delta E^{\ddagger}$ is not pH dependent. Thus, we show $\Delta E^{\ddagger}_{int}$ at pH=13 representative of the conditions for eCOR. The corresponding $\Delta E^{\ddagger}_{int}$ at CO_2R conditions (pH 7) are provided in figure S11BEP relationships (a) and intrinsic reaction barriers (b) at pH 7.figure.caption.17. Independent of pH, $\Delta E^{\ddagger}_{int}$ of C-H tends to the highest, followed by -OH and O-H. We determined average values for $\Delta E^{\ddagger}_{int}$ for each reaction type, which resulted in $\Delta E^{\ddagger}_{int}$(C-H)=1.15 eV, $\Delta E^{\ddagger}_{int}$(-OH)=0.83 eV and $\Delta E^{\ddagger}_{int}$(O-H)=0.74 eV at pH 13, emphasizing the kinetic preference towards the reduction of oxygens over carbons.

From a combination of the panels in Figure 3, two properties central to $eCO_{(2)}R$'s mechanism can be deduced: First, the endergonic thermodynamics of O-H bond formation combined with favourable kinetics is more susceptible to changes in pH. Thus, increasing the pH beyond a certain threshold will block O-H limited pathways, as either the elementary step

becomes barrierless or the subsequent step surpasses the O-H bond formation step in net barrier height. Secondly, the increased potential response of O-H leads to a preference of passing through such a step at elevated potentials. Thus, at high applied potentials, a lower amount of oxygen containing products will be produced. In summary, these two properties strengthen our finding of ethylene selectivity increasing at both intermediate pH and high applied potentials, shown in Figure 2.

Comparison to experiments strengthen the theoretical findings on potential and pH-dependence of selectivity

In order to validate our determined mechanism and selectivity behaviour for $eCO_{(2)}R$, we performed a product specific Tafel analysis on the major C_{2+}-products on literature data, which we present in Figure 4. Analogous to our previous work,[40,62] we included previously reported $eCO_{(2)}R$ polarization curves using either CO_2 (diamonds) or CO (circles) as their reactants, where we were able to determine the effective surface area corrected partial current densities (j_{ECSA}). In this analysis, we found that ethylene current densities (c.f. Figure 4(a)) exhibit a larger charge transfer coefficient (α=0.54) than the other major products, shown in panels (b)-(c). This behaviour is in agreement with our finding that O-H at the SDS has a stronger potential response. As a consequence, of the increased α, ethylene governs the C_{2+}-products at high overpotentials.

The relative increase in the transfer coefficient is about 0.15, indicating that the difference in α at the SDS is equal or a larger than this value (cf. equation 2). Interestingly, we find that the difference in transfer coefficient increases to ca. 0.22 when we consider experiments starting from CO only, mostly conducted at pH 13, as we show in figure S12Experimental database of $eCO_{(2)}R$measurements, where CO_2R and COR have been fitted separately. figure.caption.18 and is reduced to 0.08 when considering $eCO_{(2)}R$ starting from CO_2, conducted at pH 6.8. There can be a number of reasons for this observed difference, ranging from mass transport limitations in the reactor setup to changes in α with pH. Qual-

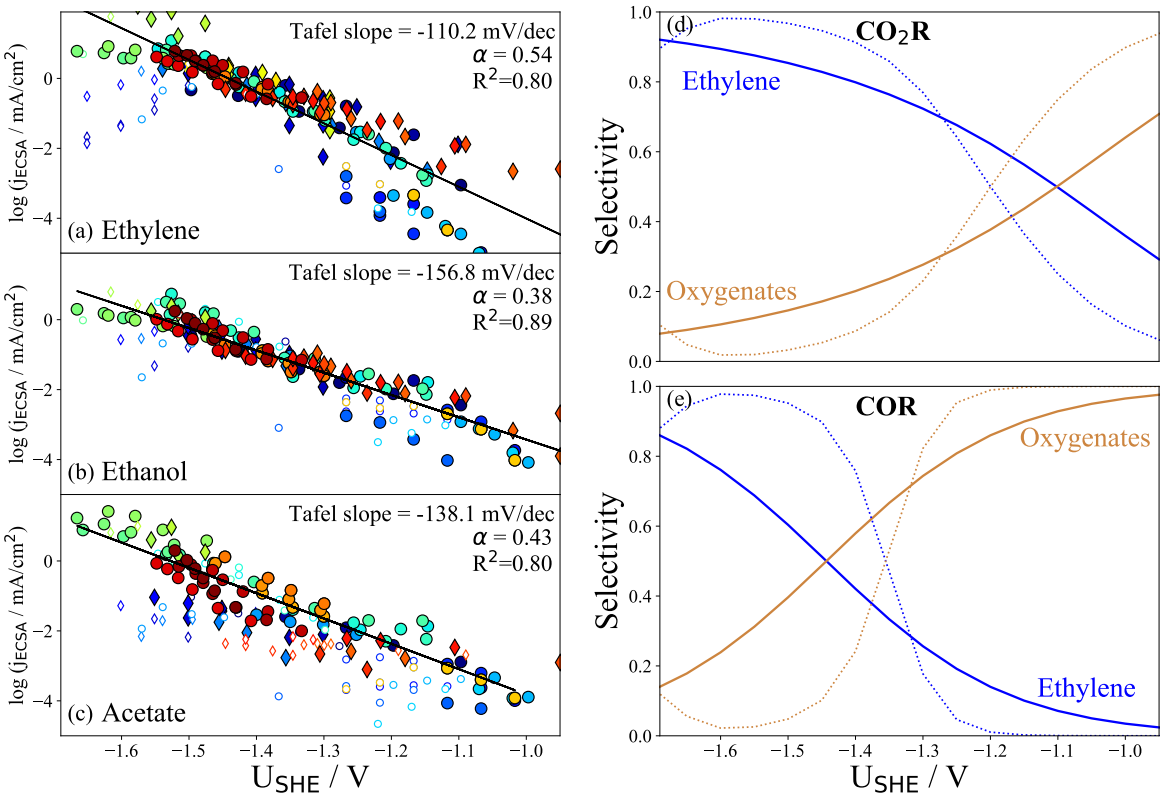

Figure 4: Tafel analysis on an experimental data collection of ECSA-corrected partial current densities towards (a) ethylene, (b) ethanol and (c) acetate resulting from CO_2R (diamonds) and COR (circles), and the resulting selectivities towards the respective products within C_{2+}-products in the case of (d) CO_2R and (e) COR. In panels (a)-(c) empty bullets represent mass transport limited currents, as determined from a deviation of the linear behaviour at high current densities. Only currents not limited by mass transport (filled bullets) have been considered in the Tafel analysis. In panels (d)-(e) the solid lines refer to the experimental trends, while our theoretical results for ethylene- (blue) and oxygenate-selectivity (black) are represented by the dotted lines.

itatively, however, it can clearly be deduced that α of ethylene production is consistently higher than the other C_{2+}-products products, independent of the reaction conditions.

We show the relative selectivity among C_{2+}-products in panels (d)-(e) of Figure 4, which we determined based on the Tafel fits performed in panels (a)-(c). Note that we use selectivity as the metric for comparison, not Faradaic efficiency, as the number of electrons needed to produce acetate is lower than for ethylene and ethanol. The selectivity for product i among the C_{2+}-products was calculated as

$$S_i^{C_{2+}} = \frac{j_{ECSA,i}/N_{e,i}}{\sum_k^{C_{2+}} j_{ECSA,k}/N_{e,k}}, \tag{4}$$

where $N_{e,i}$ refers to the number of electrons needed to produce product i. In order to show the effect of pH in more detail we chose to split between $eCO_{(2)}R$ with CO_2 and CO as reactants, respectively. When $eCO_{(2)}R$ is performed with CO_2 as the reactant we find that at low applied potentials ($\approx$-1V_{SHE}), the C_{2+}-products distribution is dominated by oxygenates. Upon increasing the potential, the distribution changes drastically, as ethylene selectivity gains from the potential throughout the potential range. Thus, it surpasses the oxygenate selectivity at -1.16V_{SHE} and reaches close to 90% selectivity within C_{2+}-products at high overpotentials.

Figure 4(e) shows, that when CO is used as the reactant in $eCO_{(2)}R$ with an electrolyte pH of 13, the selectivity change with potential is steeper than in the case of CO_2-reduction. However, the potential where the selectivity between ethylene and the oxygenate products cross is shifted to higher overpotentials, being located at -1.46V_{SHE} now.

Our theoretical selectivities, shown as dotted lines in figure 4 qualitatively reproduce both the potential and pH trends in experiments. The change in selectivity with potential is more pronounced than in experiments, while the shift with pH of the potential where ethylene starts to dominate is underestimated. A quantitative agreement was not expected and possible sources for the mismatch are an overestimation of the difference in transfer coefficient between ethylene and oxygenates and general inaccuracies in our calculated reaction kinetics

in our DFT calculations. Furthermore, the simplified statistical analysis performed on the experimental data is another source of inaccuracy for the potential where ethylene starts to govern the product distribution.

Note that at the highest potential and/or pH examined here, acetate governs the C_{2+}-products selectivity. We refer to our recent study on the mechanism towards acetate, where we describe this behaviour in detail.[40]

Guidelines for maximizing the selectivity towards specific products in experiments

Table 1: Summary of guidelines for the design of ideal reaction condition towards specific products arising from the determined mechanism and experimental analysis.

	Potential	pH	Roughness
Ethylene	**High**	**Intermediate**	Low
Ethanol	**Intermediate**	High	**High**
Acetate	**Low**/Very High	**Very High**	**Low**
Acetaldehyde	**Low**	High	**Low**
Methane	**Very high**	**Low**	High

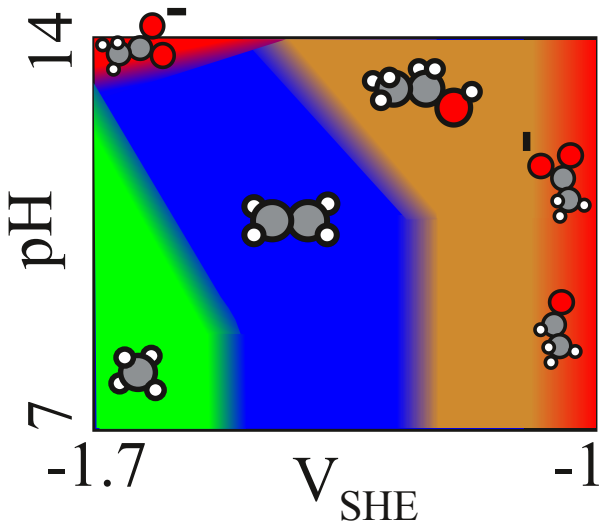

Figure 5: Summary of guidelines for the design of ideal reaction condition towards specific products arising from the determined mechanism and experimental analysis.

The combined theoretical and experimental findings lead to nearly identical conclusions for the design of electrolyzer setups for optimizing the selectivity towards specific C_{2+}-products. We summarize our identified guidelines in Table 1, based on mechanistic insights obtained from this work, our previous mechanistic studies on acetate[40] and CH_4.[62] The major design parameters used for the suggested guidelines are the applied potential, the electrolyte pH and the surface roughness. Note that in this analysis, we have not considered mass transport limitations of the reactants or products, and assume that the current densities towards the products are purely limited by the reaction kinetics. Furthermore, we do not include the ubiquitous competition with the hydrogen evolution reaction at the considered reaction conditions.

We find that the applied potential is the strongest lever to change the selectivity. Starting at low applied potentials, the first products that can be expected in $eCO_{(2)}R$ are acetate and acetaldehyde, for the same reason, i.e. both products share a SDS that consists of a competition between the adsorption/desorption equilibrium of a reaction intermediate and protonation of the intermediate, where the intermediates are H_2CCO[40,71] for acetate and acetaldehyde. The protonation suffers from low reaction rates at low applied potentials, thus making the potential-independent desorption and diffusion of the intermediates into bulk solution more likely. Upon reducing the potential below -1V_{SHE} , the protonation of *H_2CCO and acetaldehyde becomes favourable, opening up the mechanism to ethanol. Depending on the electrolyte pH, ethylene starts to dominate the selectivity between -1.2V_{SHE} (at pH 7) and -1.5V_{SHE} (at pH 13). CH_4 production, benefits the most from high applied potentials, as a consequence of it's lower Tafel slopes, particulary at high electrolyte pH.[62,72,73]

The electrolyte pH influences the competition between PCET driven CH_4 production and the *CO dimerization step. Thus, at a given intermediate absolute potential (-1V_{SHE}) and at very low (acidic) pH, or in the presence of buffer species that can efficiently donate protons, the rate towards CH_4 outcompetes *CO dimerization, as PCET steps benefit from acidic pH, while the rate towards C_{2+}-productsis unaffected by the electrolyte pH.[62,74] Increasing

the pH to neutral conditions results in the rate towards C_{2+}-products to overcome the rate for CH_4production. If the applied potential is small, oxygenates are expected to dominate the product distribution, while at potentials ¡-1.2V_{SHE} , ethylene is expected to be the dominant product. Upon increasing the pH above 11, oxygenates are found to increase their share among C_{2+}-products, since the ethylene selectivity starts to suffer from pH, discussed in detail in the previous sections and shown in Figure 2. Upon increasing the pH beyond 13, acetate starts to govern the oxygenate selectivity as it benefits from high OH^- concentrations.[40] We note that a high local pH can also be a consequence of a combination of high reduction-current densities and poor mass transport in the setup.

Finally, we also note that the roughness of the catalyst might be a tunable design parameter for steering the selectivity among oxygenate products and towards CH_4. Previously, we recognized that low catalyst roughness benefits the production of acetate, as it benefits the desorption and diffusion of *H_2CCO into bulk solution.[40] A similar argument can be made for acetaldehyde as it is produced by the same competition of an adsorption/desorption equilibrium and a PCET step on the electrode surface. Alternatively, if roughness is increased the protonation of both acetaldehyde and acetate leads to the production of ethanol. For CH_4 production previous analyses[49,62] showed that surface steps are beneficial for the kinetics of the initial protonation of *CO, as they reduce the steric hindrance in this step.

Comparison with previously proposed reaction mechanisms

We are aware that a multitude of reaction mechanisms have been proposed for the electrochemical reduction of $CO_{(2)}$ towards C_{2+}-products. In the following, we will compare our identified mechanism to (a selection of) these reaction mechanisms. We start by noting that reaction pathways that do not proceed via *CO-dimerization[47,75] are unlikely, as discussed in detail in Ref.[62]

One of the earliest complete reaction pathways towards ethylene and ethanol based on DFT-calculations was reported by Calle-Vallejo and Koper in 2013.[43] Their proposed mech-

anism based on reaction thermodynamics is comparable to ours up until the formation of *HCCO. The protonation of the central carbon in *HCCO, however, was identified as the most favourable step, owing to the highest thermodynamic stability of *HCCHO among the possible reaction intermediates (i.e.*HCCHO, *H_2CCO and *HCCOH). From this intermediate, the mechanisms towards both ethylene and ethanol proceed towards *H_2CCH_2O. The elementary steps from *H_2CCH_2O define the SDS in their proposed mechanism, with the desorption of ethylene competing with the protonation of *H_2CCH_2O towards ethanol. This SDS represents a competition between a chemical (desorption) and an electrochemical (PCET) step. Thus, only the protonation towards ethanol benefits from an increase in the potential making it the dominating product at high applied potentials. Furthermore, the SDS would exhibit only a narrow potential region (¡0.1V[38]) where both products can be observed, while at lower or higher potentials only ethylene or ethanol would be produced, respectively. In later reports by the authors,[63] the desorption of ethylene from *H_2CCH_2O has been combined with a protonation of *O in an overall electrochemical step, thereby partly addressing the issue of the above mentioned competition, but necessitating an unlikely concerted protonation and ethylene desorption step. Additionally, in contrast to Ref.,[43] we note that the (intrinsic) barriers towards *HCCHO and *H_2CCH_2O (HCC-HO and H2CCH-HO in Figure 3) are among the highest that we have calculated, rendering the pathway via *HCCHO to be energetically unfavourable. These results further highlight the importance of estimating reaction kinetics in determining the most favourable reaction pathways.

Xiao et. al proposed a mechanism towards both ethylene and ethanol including the role of adsorbed hydrogen in the mechanism.[68] This mechanism is comparable to the present work regarding the determined reaction intermediates towards ethylene, albiet with differences in the specific elementary steps. The pathway towards ethanol, however, differs drastically from the present work, as it involves the protonation of *HCCOH to *HCCHOH, which the authors recognize as being kinetically unfavourable. The ketene intermediate is not predicted as part of the mechanism in Ref.[68] and co-feeding ketene is proposed to lead to

ethylene or ethanol depending on the electrolyte pH. Our recent study on the mechanism towards acetate,[40] combined with the mechanistic analysis performed in the present study strongly suggests that ketene is a crucial intermediate towards acetate, acetaldehyde and ethanol, as only this mechanism explains the counter-intuitive enhancement of acetate with pH observed in experiments.[40] Furthermore, the participation of surface hydrogen in the mechanism might lead to strong potential and pH dependence in product selectivity. In fact, the SDS between ethylene and ethanol is identified to involve the reaction of *HCCOH to *CCH via a PCET step and surface hydrogenation of *HCCOH to *HCCHOH towards ethylene and ethanol, respectively. We argue that similar to the mechanism described in Ref.,[43] only a narrow potential window exists where both products would be produced in this competition between chemical and electrochemical steps. Furthermore, in this mechanism, the step towards ethanol would exhibit a reduction in the activity with increasing pH over the whole pH range. This behaviour would strongly alter the product distribution towards ethylene at high overpotentials, which is contrary to our findings in both the simulated mechanism and the analysis of the experimental observations detailed above.

Very recently, Peng et al. proposed selectivity pathways towards C_{2+}-productscomparable to those identified in the present study, although differing in the early stages of the reaction pathway, the potential and pH dependence of the product selectivity, and the employed computational methods.[50] First, our results clearly exclude the pathway via *HCCHO in Figure 2, a pathway found to be central to ethanol productions by Peng et al. Second, the authors identify a steep decay in the oxygenate selectivity with increasing potential which they attribute to the competition of *H-HCCO and the protonation of *HCCOH to form *CCH (+ H_2O). We identify the same behavior, but only at pH 13, while at pH 7, *HCCOH is stable enough for the OH-desorption towards *CCH to be lower in activation free energy than *HCCO-H. As a consequence of their identified reaction mechanism, the selectivity between ethylene and oxygenates is pH-dependent at all investigated pH's and the activity (as well as selectivity) towards oxygenates reduces with increasing potentials as long as

*HCC-OH limits the selectivity towards ethylene. This is a consequence of $\alpha_{\mathrm{Oxy}} \approx \alpha_{C_2H_4} - 1$, while α_{RLS} is just 0.5. Furthermore, the authors identify a lower α for *HCCO-H than for *H-HCCO, which leads to an increase of oxygenate products at high potentials in their analysis. We do not share the finding of an increase in oxygenate selectivity at high potentials both in our simulation results shown in Figure 2 or the experimental database in Figure 4. The only exception we find is the increase of acetate selectivity at very high pH,[40,71,76,77] which is consistent with our model predictions. Methodologically, we emphasize that all the reaction kinetics in the study of Peng et al. were calculated under acidic conditions using charge extrapolation to estimate charge transfer co-efficients, with H_3O+ as the proton donor. Only the use of a constant potential scheme allows the estimation of reaction kinetics in neutral/alkaline conditions with H_2O as the proton donor, without the need to include alkali cations during the NEB simulations at constant charge conditions.[42]

The selectivity to varying C_{2+}-products has often been attributed to specific faceting of the catalyst surface,[28,31,78] with Hori's seminal work[15] at the heart of the argument. We argue that a fixed facet distribution alone is not able to explain the change in product distribution with potential. However, it has been shown previously that Cu is dynamic at $eCO_{(2)}R$ conditions. Thus a change in the dominant surface facet with potential might be a viable explanation for the change in C_{2+}-products selectivity with potential, and would necessitate more thorough studies on potential-dependent surface restructuring. We emphasize that while analyzing Hori's original single crystal experiments,[15] it is crucial to consider that the measurements on the varying facets have been performed at different applied potentials. In figure S13Summary of published results measured by Hori.[15] Note that only one point per facet is given for each product and the potential vary substantially. figure.caption.19, we show a potential resolved analysis of Hori's results. Our analysis shows that all facets together actually exhibit a single trend. The most likely explanation for this trend is a restructuring of the catalyst surface under reaction conditions that results in a similar active site density on the studied single crystal surfaces.[37] Thus, we argue that attributing changes in selectivity

to nanostructuring of the catalyst surface needs to be done with care and active surface area corrected partial current densities (i.e. ECSA normalized activity) should be compared in order to avoid misleading conclusions, arising e.g. from a suppression of HER.[40] Furthermore, comparisons of varying catalyst morphologies should always be performed at similar potential and pH conditions in order to avoid selectivity changes arising from variations in the latter two parameters.

Conclusions

On the basis of constant potential DFT simulations and microkinetic modeling, we have identified reaction pathways towards ethylene and ethanol for $eCO_{(2)}R$ on Cu surfaces. Our study highlights the importance of accounting for reaction kinetics in mechanistic studies, as pathways based on reaction thermodynamics alone can lead to misleading conclusions on the preferred reaction pathway. Furthermore, the elementary reaction steps and their competition that plays a central role in determining product selectivity can be attributed to general trends in the reaction energetics for the protonation of carbon vs. oxygen species in the reaction intermediates. We find that while the protonation of oxygen species is thermodynamically less favourable than the protonation of carbon species, the reaction kinetics follows the opposite trend. Additionally, we identified a clear trend in the potential response of the respective elementary steps involving carbon vs. oxygen protonation which leads to a potential dependent selectivity between ethylene and oxygenates. We find a good agreement between the selectivity-map determined using microkinetic simulations and an experimental database which allowed us to confidently formulate guidelines for improving the selectivity in CO_2 electrolyzers towards desired $eCO_{(2)}R$ products. Furthermore, the fundamental trends identified in this work allow the a priori estimation of preferences in reaction mechanisms that can help in leveraging the current understanding for other $eCO_{(2)}R$ products and electrocatalytic processes.

Acknowledgements

The computational work leading to these results has received funding from the European Union's Horizon 2020 research and innovation program under grant agreement no. 851441, SELECTCO2, and the Villum foundation through grant no. 9455. The authors acknowledge PRACE for awarding them access to the JUWELS supercomputer at GCS@FZJ in Germany through project 2020235596.

References

(1) Malley, P. R. S., Skea, J., Slade, R., Khourdajie, A. A., van Diemen, R., McCollum, D., Pathak, M., Some, S., Vyas, P., Fradera, R., Belkacemi, M., Hasija, A., Lisboa, G., Luz, S., J.,, Eds. *Climate Change 2022: Mitigation of Climate Change Working Group III Contribution to the IPCC Sixth Assessment Report*; Cambridge University Press, Cambridge, UK and New York, NY, USA, 2022.

(2) Bushuyev, O. S.; De Luna, P.; Dinh, C. T.; Tao, L.; Saur, G.; van de Lagemaat, J.; Kelley, S. O.; Sargent, E. H. What Should We Make with CO2 and How Can We Make It? *Joule* **2018**, *2*, 825–832.

(3) Nitopi, S.; Bertheussen, E.; Scott, S. B.; Liu, X.; Engstfeld, A. K.; Horch, S.; Seger, B.; Stephens, I. E. L.; Chan, K.; Hahn, C.; Nørskov, J. K.; Jaramillo, T. F.; Chorkendorff, I. Progress and Perspectives of Electrochemical CO 2 Reduction on Copper in Aqueous Electrolyte. *Chemical Reviews* **2019**, *119*, 7610–7672.

(4) Ripatti, D. S.; Veltman, T. R.; Kanan, M. W. Carbon Monoxide Gas Diffusion Electrolysis that Produces Concentrated C2 Products with High Single-Pass Conversion. *Joule* **2019**, *3*, 2581.

(5) Nguyen, T. N.; Dinh, C.-T. Gas diffusion electrode design for electrochemical carbon dioxide reduction. *Chemical Society Reviews* **2020**,

(6) García de Arquer, F. P. et al. CO 2 electrolysis to multicarbon products at activities greater than 1 A cm -2. *Science* **2020**, *367*, 661–666.

(7) Wakerley, D.; Lamaison, S.; Wicks, J.; Clemens, A.; Feaster, J.; Corral, D.; Jaffer, S. A.; Sarkar, A.; Fontecave, M.; Duoss, E. B.; Baker, S.; Sargent, E. H.; Jaramillo, T. F.; Hahn, C. Gas diffusion electrodes, reactor designs and key metrics of low-temperature CO2 electrolysers. *Nature Energy* **2022**, *7*, 130–143.

(8) De Luna, P.; Hahn, C.; Higgins, D.; Jaffer, S. A.; Jaramillo, T. F.; Sargent, E. H. What would it take for renewably powered electrosynthesis to displace petrochemical processes? *Science* **2019**, *364*, eaav3506.

(9) Hoffman, Z. B.; Gray, T. S.; Moraveck, K. B.; Gunnoe, T. B.; Zangari, G. Electrochemical Reduction of Carbon Dioxide to Syngas and Formate at Dendritic Copper–Indium Electrocatalysts. *ACS Catalysis* **2017**, *7*, 5381–5390.

(10) Zhu, M.; Tian, P.; Li, J.; Chen, J.; Xu, J.; Han, Y.-F. Structure-Tunable Copper–Indium Catalysts for Highly Selective CO 2 Electroreduction to CO or HCOOH. *ChemSusChem* **2019**, *12*, 3955–3959.

(11) Liang, S.; Huang, L.; Gao, Y.; Wang, Q.; Liu, B. Electrochemical Reduction of CO2 to CO over Transition Metal/N-Doped Carbon Catalysts: The Active Sites and Reaction Mechanism. *Advanced Science* **2021**, *8*.

(12) Proietto, F.; Patel, U.; Galia, A.; Scialdone, O. Electrochemical conversion of CO2 to formic acid using a Sn based electrode: A critical review on the state-of-the-art technologies and their potential. *Electrochimica Acta* **2021**, *389*.

(13) Al-Tamreh, S. A.; Ibrahim, M. H.; El-Naas, M. H.; Vaes, J.; Pant, D.; Benamor, A.; Amhamed, A. Electroreduction of Carbon Dioxide into Formate: A Comprehensive Review. *ChemElectroChem* **2021**, *8*, 3207–3220.

(14) Greenblatt, J. B.; Miller, D. J.; Ager, J. W.; Houle, F. A.; Sharp, I. D. The Technical and Energetic Challenges of Separating (Photo)Electrochemical Carbon Dioxide Reduction Products. *Joule* **2018**, *2*, 381–420.

(15) Hori, Y.; Takahashi, R.; Yoshinami, Y.; Murata, A. Electrochemical Reduction of CO at a Copper Electrode. *J. Phys. Chem. B* **1997**, *101*, 7075–7081.

(16) Fan, L.; Xia, C.; Yang, F.; Wang, J.; Wang, H.; Lu, Y. Strategies in catalysts and electrolyzer design for electrochemical CO 2 reduction toward C 2+ products. *Science Advances* **2020**, *6*, eaay3111.

(17) Tang, W.; Peterson, A. A.; Varela, A. S.; Jovanov, Z. P.; Bech, L.; Durand, W. J.; Dahl, S.; Nørskov, J. K.; Chorkendorff, I. The importance of surface morphology in controlling the selectivity of polycrystalline copper for CO 2 electroreductionw. *Phys. Chem. Chem. Phys* **2012**, *14*, 76–81.

(18) Li, C. W.; Ciston, J.; Kanan, M. W. Electroreduction of carbon monoxide to liquid fuel on oxide-derived nanocrystalline copper. *Nature* **2014**, *508*, 504–507.

(19) Ren, D.; Ang, B. S.-H.; Yeo, B. S. Tuning the Selectivity of Carbon Dioxide Electroreduction toward Ethanol on Oxide-Derived Cu x Zn Catalysts. *ACS Catalysis* **2016**, *6*, 8239–8247.

(20) Varela, A. S.; Kroschel, M.; Reier, T.; Strasser, P. Controlling the selectivity of CO2 electroreduction on copper: The effect of the electrolyte concentration and the importance of the local pH. *Catalysis Today* **2016**, *260*, 8–13.

(21) Huang, Y.; Handoko, A. D.; Hirunsit, P.; Yeo, B. S. Electrochemical Reduction of CO 2 Using Copper Single-Crystal Surfaces: Effects of CO* Coverage on the Selective Formation of Ethylene. *ACS Catalysis* **2017**, *7*, 1749–1756.

(22) Hahn, C.; Hatsukade, T.; Kim, Y.-G.; Vailionis, A.; Baricuatro, J. H.; Higgins, D. C.; Nitopi, S. A.; Soriaga, M. P.; Jaramillo, T. F. Engineering Cu surfaces for the electrocatalytic conversion of CO 2 : Controlling selectivity toward oxygenates and hydrocarbons. *Proceedings of the National Academy of Sciences* **2017**, *114*, 5918–5923.

(23) Clark, E. L.; Hahn, C.; Jaramillo, T. F.; Bell, A. T. Electrochemical CO2 Reduction over Compressively Strained CuAg Surface Alloys with Enhanced Multi-Carbon Oxygenate Selectivity. *Journal of the American Chemical Society* **2017**, *139*, 15848–15857.

(24) Wang, L.; Nitopi, S. A.; Bertheussen, E.; Orazov, M.; Morales-Guio, C. G.; Liu, X.; Higgins, D. C.; Chan, K.; Nørskov, J. K.; Hahn, C.; Jaramillo, T. F. Electrochemical Carbon Monoxide Reduction on Polycrystalline Copper: Effects of Potential, Pressure, and pH on Selectivity toward Multicarbon and Oxygenated Products. *ACS Catalysis* **2018**, *8*, 7445–7454.

(25) Zhuang, T.-T. et al. Steering post-C–C coupling selectivity enables high efficiency electroreduction of carbon dioxide to multi-carbon alcohols. *Nature Catalysis* **2018**, *1*, 421–428.

(26) Wang, L.; Nitopi, S.; Wong, A. B.; Snider, J. L.; Nielander, A. C.; Morales-Guio, C. G.; Orazov, M.; Higgins, D. C.; Hahn, C.; Jaramillo, T. F. Electrochemically converting carbon monoxide to liquid fuels by directing selectivity with electrode surface area. *Nature Catalysis* **2019**, *2*, 702–708.

(27) Vasileff, A.; Zhi, X.; Xu, C.; Ge, L.; Jiao, Y.; Zheng, Y.; Qiao, S.-Z. Selectivity Control for Electrochemical CO 2 Reduction by Charge Redistribution on the Surface of Copper Alloys. *ACS Catalysis* **2019**, *9*, 9411–9417.

(28) Arán-Ais, R. M.; Scholten, F.; Kunze, S.; Rizo, R.; Roldan Cuenya, B. The role of in situ generated morphological motifs and Cu(i) species in C2+ product selectivity during CO2 pulsed electroreduction. *Nature Energy* **2020**, *5*, 317–325.

(29) De Gregorio, G. L.; Burdyny, T.; Loiudice, A.; Iyengar, P.; Smith, W. A.; Buonsanti, R. Facet-Dependent Selectivity of Cu Catalysts in Electrochemical CO 2 Reduction at Commercially Viable Current Densities. *ACS Catalysis* **2020**, *10*, 4854–4862.

(30) Wang, X.; Klingan, K.; Klingenhof, M.; Möller, T.; Ferreira de Araújo, J.; Martens, I.; Bagger, A.; Jiang, S.; Rossmeisl, J.; Dau, H.; Strasser, P. Morphology and mechanism of highly selective Cu(II) oxide nanosheet catalysts for carbon dioxide electroreduction. *Nature Communications* **2021**, *12*, 794.

(31) Huang, Y.; Handoko, A. D.; Hirunsit, P.; Yeo, B. S. Electrochemical Reduction of CO 2 Using Copper Single-Crystal Surfaces: Effects of CO* Coverage on the Selective Formation of Ethylene. *ACS Catalysis* **2017**, *7*, 1749–1756.

(32) Kim, D.; Resasco, J.; Yu, Y.; Asiri, A. M.; Yang, P. Synergistic geometric and electronic effects for electrochemical reduction of carbon dioxide using gold–copper bimetallic nanoparticles. *Nature Communications* **2014**, *5*, 4948.

(33) Riyanto,; Ramadan, S.; Fariduddin, S.; Aminudin, A. R.; Hayatri, A. K. Conversion of Carbon Dioxide into Ethanol by Electrochemical Synthesis Method Using Cu-Zn Electrode. *IOP Conference Series: Materials Science and Engineering* **2018**, *288*, 012136.

(34) Ma, M.; Hansen, H. A.; Valenti, M.; Wang, Z.; Cao, A.; Dong, M.; Smith, W. A. Electrochemical reduction of CO 2 on compositionally variant Au-Pt bimetallic thin films. *Nano Energy* **2017**,

(35) Ting, L. R. L.; Piqué, O.; Lim, S. Y.; Tanhaei, M.; Calle-Vallejo, F.; Yeo, B. S. Enhancing CO 2 Electroreduction to Ethanol on Copper–Silver Composites by Opening an Alternative Catalytic Pathway. *ACS Catalysis* **2020**, *10*, 4059–4069.

(36) Lee, S. H.; Sullivan, I.; Larson, D. M.; Liu, G.; Toma, F. M.; Xiang, C.; Drisdell, W. S. Correlating Oxidation State and Surface Area to Activity from Operando Studies of

Copper CO Electroreduction Catalysts in a Gas-Fed Device. *ACS Catalysis* **2020**, *10*, 8000–8011.

(37) Lee, S. H.; Lin, J. C.; Farmand, M.; Landers, A. T.; Feaster, J. T.; Avilés Acosta, J. E.; Beeman, J. W.; Ye, Y.; Yano, J.; Mehta, A.; Davis, R. C.; Jaramillo, T. F.; Hahn, C.; Drisdell, W. S. Oxidation State and Surface Reconstruction of Cu under CO 2 Reduction Conditions from In Situ X-ray Characterization. *Journal of the American Chemical Society* **2021**, *143*, 588–592.

(38) Govindarajan, N.; Kastlunger, G.; Heenen, H. H.; Chan, K. Improving the intrinsic activity of electrocatalysts for sustainable energy conversion: where are we and where can we go? *Chemical Science* **2022**, *13*, 14–26.

(39) Christensen, O.; Zhao, S.; Sun, Z.; Bagger, A.; Lauritsen, J. V.; Steen, P. U.; Daasbjerg, K.; Rossmeisl, J. Selectivity and Intrinsic Activity of Functionalized Cu Surfaces: Can the CO2 Reduction Reaction be Improved on Cu? **2022**,

(40) Heenen, H. H.; Shin, H.; Kastlunger, G.; Overa, S.; Gauthier, J. A.; Jiao, F.; Chan, K. The mechanism for acetate formation in electrochemical CO (2) reduction on Cu: selectivity with potential, pH, and nanostructuring. *Energy & Environmental Science* **2022**, *15*, 3978–3990.

(41) Nørskov, J. K.; Studt, F.; Abild-Pedersen, F.; Bligaard, T. *Fundamental Concepts in Heterogeneous Catalysis*; John Wiley & Sons, Inc: Hoboken, NJ, USA, 2014; pp 155–174.

(42) Lamoureux, P. S.; Singh, A. R.; Chan, K. pH Effects on Hydrogen Evolution and Oxidation over Pt(111): Insights from First-Principles. *ACS Catalysis* **2019**, *9*, 6194–6201.

(43) Calle-Vallejo, F.; Koper, M. T. M. Theoretical Considerations on the Electroreduction

of CO to C 2 Species on Cu(100) Electrodes. *Angewandte Chemie International Edition* **2013**, *52*, 7282–7285.

(44) Schouten, K. J. P.; Qin, Z.; Pérez Gallent, E.; Koper, M. T. M. Two Pathways for the Formation of Ethylene in CO Reduction on Single-Crystal Copper Electrodes. *Journal of the American Chemical Society* **2012**, *134*, 9864–9867.

(45) Wang, X.; de Araújo, J. F.; Ju, W.; Bagger, A.; Schmies, H.; Kühl, S.; Rossmeisl, J.; Strasser, P. Mechanistic reaction pathways of enhanced ethylene yields during electroreduction of CO2–CO co-feeds on Cu and Cu-tandem electrocatalysts. *Nature Nanotechnology* **2019**, *14*, 1063–1070.

(46) Birdja, Y. Y.; Pérez-Gallent, E.; Figueiredo, M. C.; Göttle, A. J.; Calle-Vallejo, F.; Koper, M. T. M. Advances and challenges in understanding the electrocatalytic conversion of carbon dioxide to fuels. *Nature Energy* **2019**, *4*, 732–745.

(47) Garza, A. J.; Bell, A. T.; Head-Gordon, M. Mechanism of CO 2 Reduction at Copper Surfaces: Pathways to C 2 Products. *ACS Catalysis* **2018**, *8*, 1490–1499.

(48) Liu, S. P.; Zhao, M.; Gao, W.; Jiang, Q.; Jacob, T. Theoretical Studies on the CO2 Reduction to CH3OH on Cu(211). *Electrocatalysis* **2017**, *8*, 647–656.

(49) Liu, X.; Schlexer, P.; Xiao, J.; Ji, Y.; Wang, L.; Sandberg, R. B.; Tang, M.; Brown, K. S.; Peng, H.; Ringe, S.; Hahn, C.; Jaramillo, T. F.; Nørskov, J. K.; Chan, K. pH effects on the electrochemical reduction of CO (2) towards C 2 products on stepped copper. *Nature Communications* **2019**, *10*, 1–10.

(50) Peng, H.-J.; Tang, M. T.; Halldin Stenlid, J.; Liu, X.; Abild-Pedersen, F. Trends in oxygenate/hydrocarbon selectivity for electrochemical CO(2) reduction to C2 products. *Nature Communications* **2022**, *13*, 1399.

(51) Bockris, J. O.; Nagy, Z. Symmetry factor and transfer coefficient. A source of confusion in electrode kinetics. *Journal of Chemical Education* **1973**, *50*, 839.

(52) Guidelli, R.; Compton, R. G.; Feliu, J. M.; Gileadi, E.; Lipkowski, J.; Schmickler, W.; Trasatti, S. Defining the transfer coefficient in electrochemistry: An assessment (IUPAC Technical Report). *Pure and Applied Chemistry* **2014**, *86*, 245–258.

(53) Ringe, S.; Morales-guio, C. G.; Chen, L. D.; Jaramillo, T. F.; Chan, K. Double layer charging driven CO 2 adsorption limits the rate of electrochemical CO 2 reduction on Au. **2019**, 1–12.

(54) Limaye, A. M.; Zeng, J. S.; Willard, A. P.; Manthiram, K. Bayesian data analysis reveals no preference for cardinal Tafel slopes in CO2 reduction electrocatalysis. *Nature Communications* **2021**, *12*, 703.

(55) Patel, A. M.; Vijay, S.; Kastlunger, G.; Nørskov, J. K.; Chan, K. Generalizable Trends in Electrochemical Protonation Barriers. *The Journal of Physical Chemistry Letters* **2021**, *12*, 5193–5200.

(56) Lozovoi, A. Y.; Alavi, A.; Kohanoff, J.; Lynden-Bell, R. M. Ab initio simulation of charged slabs at constant chemical potential. *The Journal of Chemical Physics* **2001**, *115*, 1661–1669.

(57) Sundararaman, R.; Schwarz, K. Evaluating continuum solvation models for the electrode-electrolyte interface: Challenges and strategies for improvement. *The Journal of Chemical Physics* **2017**, *146*, 84111.

(58) Sundararaman, R.; GoddardIII, W. A.; Arias, T. A. Grand canonical electronic density-functional theory: Algorithms and applications to electrochemistry. *The Journal of Chemical Physics* **2017**, *146*, 114104.

(59) Kastlunger, G.; Lindgren, P.; Peterson, A. A. Controlled-Potential Simulation of Elementary Electrochemical Reactions: Proton Discharge on Metal Surfaces. *The Journal of Physical Chemistry C* **2018**, *122*, 12771–12781.

(60) Melander, M. M.; Kuisma, M. J.; Christensen, T. E. K.; Honkala, K. Grand-canonical approach to density functional theory of electrocatalytic systems: Thermodynamics of solid-liquid interfaces at constant ion and electrode potentials. *The Journal of Chemical Physics* **2019**, *150*, 041706.

(61) Hörmann, N. G.; Reuter, K. Thermodynamic Cyclic Voltammograms Based on Ab Initio Calculations: Ag(111) in Halide-Containing Solutions. *Journal of Chemical Theory and Computation* **2021**, *17*, 1782–1794.

(62) Kastlunger, G.; Wang, L.; Govindarajan, N.; Heenen, H. H.; Ringe, S.; Jaramillo, T.; Hahn, C.; Chan, K. Using pH Dependence to Understand Mechanisms in Electrochemical CO Reduction. *ACS Catalysis* **2022**, *12*, 4344–4357.

(63) Kortlever, R.; Shen, J.; Schouten, K. J. P.; Calle-Vallejo, F.; Koper, M. T. M. Catalysts and Reaction Pathways for the Electrochemical Reduction of Carbon Dioxide. *The Journal of Physical Chemistry Letters* **2015**, *6*, 4073–4082.

(64) Iyengar, P.; Kolb, M. J.; Pankhurst, J. R.; Calle-Vallejo, F.; Buonsanti, R. Elucidating the Facet-Dependent Selectivity for CO 2 Electroreduction to Ethanol of Cu–Ag Tandem Catalysts. *ACS Catalysis* **2021**, *11*, 4456–4463.

(65) Piqué, O.; Low, Q. H.; Handoko, A. D.; Yeo, B. S.; Calle-Vallejo, F. Selectivity Map for the Late Stages of CO and CO2 Reduction to C2 Species on Copper Electrodes. *Angewandte Chemie International Edition* **2021**, *60*, 10784–10790.

(66) Bertheussen, E.; Verdaguer-Casadevall, A.; Ravasio, D.; Montoya, J. H.; Trimarco, D. B.; Roy, C.; Meier, S.; Wendland, J.; Nørskov, J. K.; Stephens, I. E. L.;

Chorkendorff, I. Acetaldehyde as an Intermediate in the Electroreduction of Carbon Monoxide to Ethanol on Oxide-Derived Copper. *Angewandte Chemie International Edition* **2016**, *55*, 1450–1454.

(67) Chang, X.; Malkani, A.; Yang, X.; Xu, B. Mechanistic Insights into Electroreductive C-C Coupling between CO and Acetaldehyde into Multicarbon Products. 2020.

(68) Xiao, H.; Cheng, T.; Goddard, W. A.; Sundararaman, R. Mechanistic Explanation of the pH Dependence and Onset Potentials for Hydrocarbon Products from Electrochemical Reduction of CO on Cu (111). *Journal of the American Chemical Society* **2016**, *138*, 483–486.

(69) Jónsson, H.; Mills, G.; Jacobsen, K. W. In *Classical and Quantum Dynamics in Condensed Phase Simulations*; Berne, B. J., Ciccotti, G., Coker, D. F., Eds.; World Scientific, 1998; Vol. 385.

(70) Lindgren, P.; Kastlunger, G.; Peterson, A. A. A Challenge to the G $\sim$ 0 Interpretation of Hydrogen Evolution. *ACS Catalysis* **2019**, *10*, 121–128.

(71) Ma, M.; Deng, W.; Xu, A.; Hochfilzer, D.; Qiao, Y.; Chan, K.; Chorkendorff, I.; Seger, B. Local reaction environment for selective electroreduction of carbon monoxide. *Energy & Environmental Science* **2022**, *15*, 2470–2478.

(72) Li, J.; Chang, X.; Zhang, H.; Malkani, A. S.; Cheng, M.-j.; Xu, B.; Lu, Q. Electrokinetic and in situ spectroscopic investigations of CO electrochemical reduction on copper. *Nature Communications* **2021**, *12*, 3264.

(73) Chang, X.; Li, J.; Xiong, H.; Zhang, H.; Xu, Y.; Xiao, H.; Lu, Q.; Xu, B. C-C Coupling Is Unlikely to Be the Rate-Determining Step in the Formation of C2+ Products in the Copper-Catalyzed Electrochemical Reduction of CO. *Angewandte Chemie International Edition* **2021**,

(74) Hochfilzer, D.; Xu, A.; Sørensen, J. E.; Needham, J. L.; Krempl, K.; Toudahl, K. K.; Kastlunger, G.; Chorkendorff, I.; Chan, K.; Kibsgaard, J. Transients in Electrochemical CO Reduction Explained by Mass Transport of Buffers. *ACS Catalysis* **2022**, *12*, 5155–5161.

(75) Nie, X.; Esopi, M. R.; Janik, M. J.; Asthagiri, A. Selectivity of CO2 reduction on copper electrodes: The role of the kinetics of elementary steps. *Angewandte Chemie - International Edition* **2013**, *52*, 2459–2462.

(76) Jouny, M.; Luc, W.; Jiao, F. High-rate electroreduction of carbon monoxide to multi-carbon products. *Nature Catalysis* **2018**, *1*, 748–755.

(77) Luc, W.; Fu, X.; Shi, J.; Lv, J.-J.; Jouny, M.; Ko, B. H.; Xu, Y.; Tu, Q.; Hu, X.; Wu, J.; Yue, Q.; Liu, Y.; Jiao, F.; Kang, Y. Two-dimensional copper nanosheets for electrochemical reduction of carbon monoxide to acetate. *Nature Catalysis* **2019**, *2*, 423–430.

(78) Bagger, A.; Ju, W.; Varela, A. S.; Strasser, P.; Rossmeisl, J. Electrochemical CO 2 Reduction: Classifying Cu Facets. *ACS Catalysis* **2019**, *9*, 7894–7899.